INTERNATIONAL JOURNAL FOR NUMERICAL METHODS IN ENGINEERING

Int. J. Numer. Meth. Engng 2011; **00**:1–35

Published online in Wiley InterScience (www.interscience.wiley.com). DOI: 10.1002/nme

3D Domain Decomposition for Violent Wave-Ship Interactions

M. Greco[1,2,3,*], G. Colicchio[1,2], C. Lugni[1,2] and O.M. Faltinsen[2,3]

[1] *CNR-INSEAN, The Italian Ship Model Basin, via di Vallerano 139, 00128 Roma - Italy.* [2] *Centre for Ships and Ocean Structures, NTNU, Trondheim - Norway.* [3] *Dept. of Marine Hydrodynamics, NTNU, Trondheim - Norway*

SUMMARY

A 3D Domain-Decomposition (DD) strategy has been developed to deal with violent wave-ship interactions involving water on deck and slamming occurrence. It couples a linear potential-flow seakeeping solver with a Navier-Stokes (NS) method. The latter is applied in an inner domain where slamming, water on deck, free-surface fragmentation may occur, involving important flow nonlinearities. The field solver combines an approximated Projection method with a Level-Set technique for the free-surface evolution. A hybrid strategy, combining the Eulerian Level-Set concept to Lagrangian markers, is used to enforce more accurately the body-boundary condition in case of high local curvatures. Main features of the weak and strong coupling algorithms are described with special focus on the boundary conditions for the inner solver. Two ways of estimating the nonlinear loads by the NS method are investigated, based on an extrapolation technique and an interpolation marching cube algorithm, respectively. The DD is applied for the case of a freely-floating patrol ship in head-sea regular waves and compared against water-on-deck experiments in terms of flow evolution, body motions, pressure on the hull. Improvement of the solver efficiency and accuracy are suggested.

Received . . .

KEY WORDS: 3D domain-decomposition; weak/strong coupling; linear potential theory; Navier-Stokes solver; level-set; hybrid technique; violent wave-body interactions

*Correspondence to: CNR-INSEAN, via di Vallerano 139, 00128 Roma - Italy or CeSOS/NTNU, O. Nielsens vei 10, 7491 Trondheim - Norway. E-mail: marilena.greco@cnr.it; marilena.greco@ntnu.no

1. INTRODUCTION

Violent wave-vessel interactions may cause nonlinear phenomena relevant for the local and/or global behavior of the structure, depending on the vehicle size relative to the waves and on the working conditions. In this context, water shipping and slamming represent an important issue at design stage. They are also relevant in fixing the proper operational limits of the vessels. Nowadays model tests represent still the most reliable tool for this type of investigations but the costs remain high. As a result, carrying on systematic analyses is almost prohibitive and in general one must limit the analysis to the examination of the most critical conditions only. On the other hand the computer power is continuously increasing and the Computational Fluid Dynamics (CFD) methods are growing quickly. In the seakeeping field they need still an important assessment work in terms of verification and validation and they are still too time consuming to provide, in a feasible time, information about the behavior at sea of a vessel with generally complex geometry. The numerical research effort is therefore focused on filling the gap in terms of reliability and developing efficient and robust solvers. The authors have proposed in the past a Domain-Decomposition (DD) approach (see [1] and [2]) as a possible compromise between capability in handling the most relevant phenomena, accuracy in estimating the physical quantities of interest, and efficiency. The method was implemented as two-dimensional and showed promising results when compared to reference solutions and experiments. The idea is to split the problem into sub-domains, say two, and use in each of them the most efficient solver, as long as suitable and accurate. In particular, the implemented DD used a Navier-Stokes solver able to handle large deformations, breaking and fragmentation of the free surface, air entrapment and impact events, in an inner domain where violent water-vessel interactions could occur. The method combines a Finite-Difference scheme with a Level-Set technique to capture the free-surface evolution. In a remaining outer domain, where the water behaves as inviscid and irrotational, a nonlinear potential-flow solver based on a Boundary Element Method (BEM) was adopted.

Here we consider a step forward of that activity. The effort is to include 3D effects and to overcome the implementation issues connected with them. The application is the 3D seakeeping

Prepared using nmeauth.cls
DOI: 10.1002/nme

problem of a vessel without forward speed and in regular deep-water head sea waves. This is relevant for Floating Production Storage and Offloading (FPSO) ships which are used as oil platforms and are typically weather vanying which means that head-sea waves represent the most critical conditions. The numerical solver is a DD strategy splitting the problem into an inner domain where violent wave-body interactions can occur and an outer domain where the free surface remains smooth on a large scale and linear (or weakly nonlinear) potential flow theory can be applied to capture the relevant flow features. In our case the inner domain can be identified in a sea portion containing the forward portion of the ship because there the body motions will be the largest and slamming and water shipping phenomena are likely to occur. The rest of the sea domain can be considered as outer domain, *i.e.* with dominant potential flow features. The inner domain is solved by a Navier-Stokes method developed as an extension of that applied in 2D flow conditions, the outer domain is handled by a potential-flow solver. In the present implementation in general nonlinear effects are neglected in the outer domain. This has the advantage of using the frequency-domain approach avoiding the need for solving in time the outer-domain problem, with great saving of computational cost. With this, all the features of the solver can be assessed step-by-step. Later more complicated modellings of the flow can be included. The solution algorithm is described in the next sections in terms of the two adopted solvers and of the DD strategy coupling them, then the seakeeping problem of a patrol ship at rest in regular head-sea waves is examined and a validation is performed by comparing against the corresponding model tests. Eventually, the main conclusions and future steps are outlined.

2. COUPLED METHODS: OUTER SOLVER

Here the water is assumed as incompressible, inviscid and in irrotational motion. Air and nonlinear effects are neglected. So the global seakeeping problem for a marine vehicle at rest and in head-sea deep-water waves is solved within the linear potential flow theory. The frequency-domain solver documented in [3] is used for this purpose. Because the basic theory and the solution technique are very well established and can be found in text books, e.g. [4], here only the main features are recalled. The method solves the problem by using the variable-separation strategy for the

Prepared using nmeauth.cls
DOI: 10.1002/nme

velocity potential, *i.e.* $\phi(\boldsymbol{P},t)=\Re\{[\sum_{i=1}^{6}\dot{\xi}_i\varphi_i(\boldsymbol{P})+A(\varphi_0(\boldsymbol{P})+\varphi_7(\boldsymbol{P}))]e^{i\omega t}\}$, with t the time, $\boldsymbol{P}$ the position, φ_i the velocity potential associated with unitary velocity $\dot{\xi}_i$ of the i-th rigid degree of freedom ξ_i, and φ_0 and φ_7 are, respectively, the spatial incident-wave and scattering velocity potential per unitary wave amplitude. Further, A and $\omega=2\pi/T$ are the incident-wave amplitude and frequency. Each radiation problem and the diffraction problem are characterized by the Laplace equation, the combined free-surface condition, the radiation condition, the bottom condition, and the corresponding body impermeability condition. They are solved using the Green's second identity and the Green function solving exactly the free-surface, bottom and radiation conditions. This means that only the mean-wetted body surface must be discretized and the integral representation provides the velocity potential everywhere in the fluid domain. From this, the velocity and pressure field and the free surface elevation caused by the wave-body interaction for a given frequency ω can be estimated. The integrated loads on the vessel are obtained as added-mass, damping and restoring terms from the radiation problem and as excitation loads from the diffraction problem. Actually, the radiation and diffraction problems must be solved for several values of ω spanning from very small to very large values because the equation of motions in the coupled problem must be solved in time domain. As discussed in section 4, using the Cummins [5] and Ogilvie's [6] approach, the radiation loads are characterized by convolution integrals involving the impulse response functions and the time derivative of the rigid motions. This means that added mass (or damping) coefficients must be available strictly speaking for $\omega\in(0,\infty)$. The numerical problems associated with occurrence of irregular frequencies are overcome as in [3].

3. COUPLED METHODS: INNER SOLVER

Here the water is assumed as incompressible, viscous and in laminar conditions, the temperature is assumed uniform and constant, and the surface-tension and air effects on the liquid evolution are neglected. It means that the governing equations are the conservation of fluid mass and of fluid momentum for the unknowns velocity $\boldsymbol{u}$ and pressure p. They are solved in time, for given initial and boundary conditions, by a Navier-Stokes solver based on an approximated Projection method. A

Prepared using nmeauth.cls
DOI: 10.1002/nme

Finite-Difference scheme is adopted on a Earth-fixed Cartesian grid and combined with a Predictor-Corrector scheme for the time integration. The grid is staggered with the scalar variables defined at the cell center and the velocity components on the grid faces. The method is accurate to the second order in time and space and involves the solution of a pressure Poisson equation for each sub-set of the time-integration algorithm. The details of the solver can be found in [7]. The use of an Eulerian approach makes it necessary an additional technique to follow the evolution of the free surface and enforce the boundary condition along moving bodies.

3.1. Free surface: Level-Set technique and solution extension in air

For the free surface, a Level-Set (LS) technique is adopted which means that a with-sign normal distance function ϕ is defined (negative in water and positive in air) from the free surface. It is evolved in time as a fluid property using a second-order Euler time scheme. The details of the adopted technique can be found in [7] and [8], where the numerical choices made have been identified through careful parameter investigations in order to reduce the computational costs and preserve the physical and accurate behavior of the solution. Here the major features are recalled, in particular those relevant for the present DD solver.

To save computational time ϕ is correctly defined within a distance $\pm 6\Delta x$ from the free surface. For larger distances it is kept constant and equal to $\pm 6\Delta x$. In a narrow layer across the free surface, $\pm 2\Delta x$, the fluid properties are forced to smoothly vary from the water to the air properties, using the distance ϕ from the surface. This is necessary to prevent numerical instability but implies that the free surface is actually a layer instead of a sharp surface. The latter is recovered as $\Delta x \to 0$. The smoothing law is chosen as an exponential of a sinusoidal function (see [9]). Once the instantaneous ϕ distribution is known, the NS equations can be stepped forward in time. As said, the used solver is a one-fluid solver which means that only the water evolution is correctly described. On the other hand, the estimate of spatial gradients on a fixed Cartesian grid requires in general information at grid points in air and near the free surface (see sketch in figure 1). This means that the solution must be suitably extended to the air domain to avoid numerical instability and preserve the solver accuracy. In this framework, one can distinguish two conditions: without and with a surface-piercing

Prepared using nmeauth.cls
DOI: 10.1002/nme

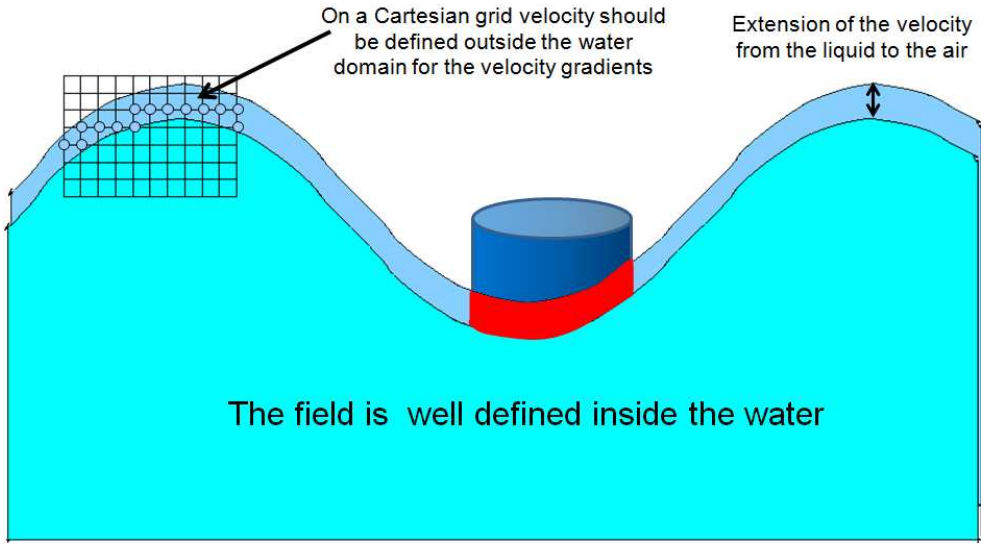

Figure 1. Eulerian one-fluid NS solver: solution extension in air.

body. In both cases the NS solution is estimated up to one and half cell in the air, *i.e.* at $\phi = 1.5\Delta x$. In the first case Colicchio [8] found that a constant extension from $\phi = 0.5\Delta x$ to the air is enough. When a surface-piercing body is present, this can cause the formation of a fictitious vorticity at the intersection between the body and the free surface, as shown in figure 2. As long as no body

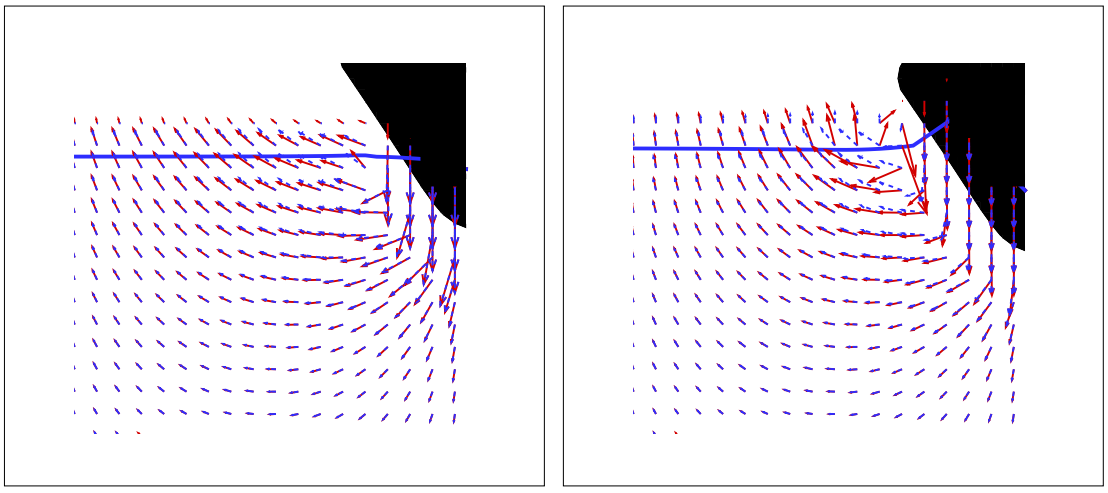

Figure 2. 2D ship cross-section forced to oscillate in heave in otherwise calm water: NS free-surface and velocity vectors. Time increases from left to right. Solid lines: velocity extension from outside the water domain. Dashed lines: velocity extension from inside the water domain. NS discretization $\Delta x = \Delta z = 0.012D$ with D the cross-section draft.

Prepared using nmeauth.cls
DOI: 10.1002/nme

is present, the air is driven by the water and the extension from above the free surface is suitable. As soon as the thin layer of air interacts with the body, such an extension is not plausible and an extension from inside the water (at least $\phi = -0.5\Delta x$) is required. In our application to a DD strategy for a 3D seakeeping problem, the constant extension of the solution from water to air leads to a more robust and physical solution but, for a given discretization, it reduces the numerical accuracy with respect to the case with constant extension from air to air. To improve the accuracy and preserve a physical flow evolution, the solution is not extended constantly from water to air but a weighting function is applied as shown in the sketch of figure 3. In our approach, the local velocity

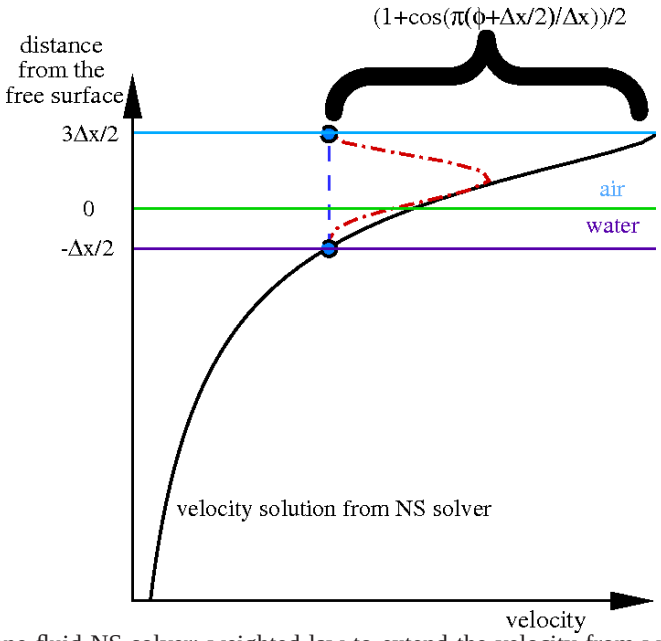

Figure 3. Eulerian one-fluid NS solver: weighted law to extend the velocity from water to air in the DD strategy.

solution (solid line) is multiplied by the weighting function $1/2\{1 + \cos[\pi(\phi + 0.5\Delta x)/\Delta x]\}$ so that the actual velocity profile is given by the dash-dotted line. It means that at $\phi = 1.5\Delta x$ the velocity is equal to the NS value at $\phi = -0.5\Delta x$ (dashed line) and for $-0.5\Delta x < \phi < 1.5\Delta x$ is between the local NS solution and the constant extension value from $\phi = -0.5\Delta x$.

3.2. Body-boundary condition: hybrid technique

The body-boundary condition is approximated as

Prepared using nmeauth.cls
DOI: 10.1002/nme

$$\boldsymbol{u} = s(\phi_{body})\boldsymbol{u}_B + [1 - s(\phi_{body})]\boldsymbol{u}_F \tag{1}$$

where $\boldsymbol{u}_F$ and $\boldsymbol{u}_B$ are, respectively, the fluid and body velocity and $s(\phi_{body})$ is a function defining the position of the body. If $s(\phi_{body})$ is a step function, unitary in the body and null in the fluid, then the boundary condition would be exactly satisfied. In this work, for computation reasons, $s(\phi_{body})$ is substituted with a smoothed function.

For the solid boundary a hybrid technique is applied (see figure 4). This approach comes from the idea in [10] but the present implementation follows the work by Colicchio [8]. Here the major features are briefly outlined. The method combines the Eulerian Level-Set technique with Lagrangian markers and is useful when the body geometry presents locally high curvatures or singularities. In these circumstances, the classical advection of a Level-Set function would smooth out the details of the body geometry and lead to greater numerical errors in the local enforcement of the body-boundary condition. Rather than deforming locally or regridding in time the mesh, a level-set ϕ_{body} (positive in fluid, negative in the body) is used to transfer the body-boundary condition at the collocation points of the numerical fixed grid. In this way it is not necessary to deform locally, or regrid, in time the mesh to follow the body motion. Within the hybrid strategy, the Level-Set function is defined through the Lagrangian markers, they are body particles initially defined on a uniform grid four times finer than the minimum mesh size in the computational grid and within a band across the body surface six times larger than the maximum mesh size of the computational grid. The related value of ϕ_{body} is estimated at the initial time and followed in time through the markers moving with the body. Their values are used to interpolate the ϕ_{body} value at the current time instant. To prevent that interpolation errors could affect the accuracy of the Level-Set function definition, only the values between $-3\Delta x$ and $3\Delta x$ are preserved. At larger distances from the body surface, the threshold value of $3\Delta x$ is assumed with the consistent sign. This approach results in a more accurate solution for a given mesh size but also leads to an increased computational time with a factor about 5. Such additional cost can be reduced using information from the local topology. For example, within a time step Δt the particles can not move more than $\alpha\Delta\boldsymbol{x}$ (with $\alpha < 1$), so

Prepared using nmeauth.cls
DOI: 10.1002/nme

the initialization of the Level-Set function ϕ_{body} is needed to be performed just in a subset of cells crossed by the markers.

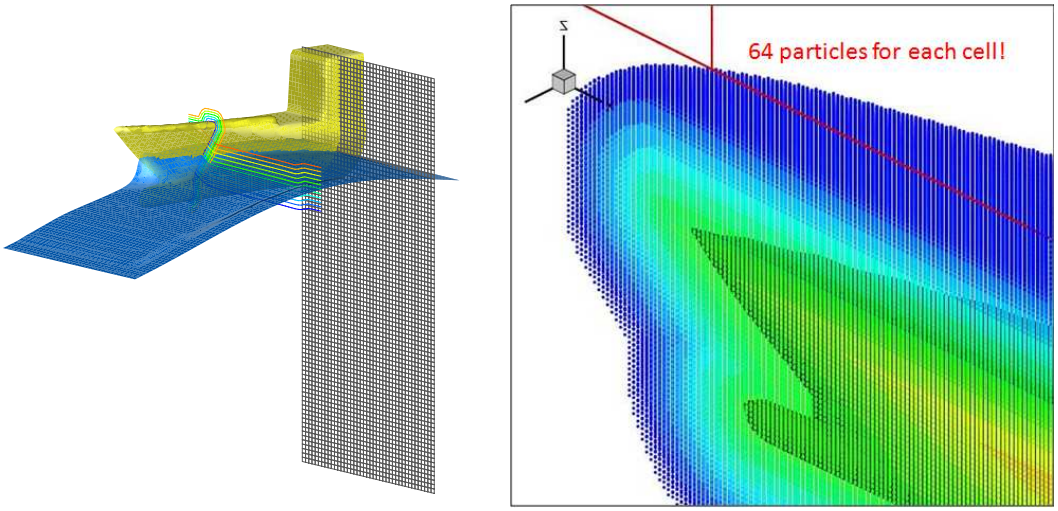

Figure 4. NS solver: fixed Cartesian grid and Level-Set technique for the free surface and the body (left), and Lagrangian markers to improve the body description (right).

3.3. Hull loads estimations: extrapolation and interpolation algorithms

Within the adopted Eulerian NS solver, the pressure is defined up to a cell across the body surface $\phi_{body} = 0$, but it is not directly available along $\phi_{body} = 0$. It means that a proper numerical algorithm must be identified to estimate the loads on the body. This is a common problem for methods using embedded grids, while those applying boundary-fitted grids can directly integrate the pressure available from the solution along the body surface. Colicchio [8] identified two possible methods to estimate the loads: (1) the first approximates the surface integrals for the loads as a volume integral introducing an approximated Dirac-Delta function and then estimates the loads on the body surface as a parabolic extrapolation from the loads estimated at three ϕ_{body} iso-surfaces, at 0.5, 1 and 1.5 Δx from the body surface; (2) the second approach interpolates the pressure along the body surface discretized in triangles and then integrates along each triangle. The triangles are identified at any needed time instant through the marching-cube scheme which searches the triangular intersection of each grid cell with the body surface among fifteen possible scenarios per direction. The second method was found more accurate and free from numerical oscillations occurring when using the first

Prepared using nmeauth.cls
DOI: 10.1002/nme

approach in the case of body motions and induced by errors in extrapolating p not exactly normally to the body surface. Therefore it is used here. The negative aspect is CPU-time requirements greater of at least a factor four with respect to the first method. To limit the computational cost, the more efficient version proposed by Colicchio [8] can be applied. In this case, the triangles are found once for all at the first time instant and then moved in time rigidly with the body. This means that the triangles are not any longer the intersections of the computational cells with the body surface, but generally crossing the grid. To maintain high accuracy, in this case the triangles are found at the initial time using the marching-cube algorithm on the grid adopted to define the Lagrangian markers. Such grid is four times finer than the computational grid.

4. DOMAIN-DECOMPOSITION STRATEGY: WEAK AND STRONG COUPLING

We assume the 3D seakeeping problem of a vessel without forward speed and in regular deep-water head-sea waves and investigate this by means of a Domain-Decomposition (DD) strategy. We identify an inner domain in a sea area containing the forward portion of the ship and the rest of the fluid domain is considered as outer domain. The outer and inner domains are solved, respectively, by the potential-flow solver and the Navier-Stokes method explained in the previous two sections. Within the DD the information is exchanged between the two domains in time. When the information travels in one direction only, *i.e.* from the outer to the inner domain, the coupling is called weak or one directional. When the information goes back and forth between the two domains, the coupling is named strong. By information we may mean local and/or global quantities. Colicchio *et al.* [1] investigated a 2D strong-coupling algorithm where the information was given in terms of local quantities: pressure, velocity and free surface elevation, exchanged between the two domains. Here the information is still given in terms of such variables when going from the outer to the inner domain while the information is provided in terms of global quantities when traveling from the inner to the outer domain. This implies in a way a relaxation of the performed coupling and leads to saving computational time. The inner solution provides the body loads estimated by the Navier-Stokes solver on a body portion always inside the inner domain. They are summed to the body loads

Prepared using nmeauth.cls
DOI: 10.1002/nme

estimated in the rest of the body surface by the potential-flow solver and the resulting loads are used to estimate the body motions in time. Obviously the loads depend on the motions, as well as on the body velocity and acceleration and on the body wetted surface. The rigid-body motion equations are given by the Newton's second law and are written here along the body coordinate frame (X, Y, Z) so that the ship generalized mass matrix $\boldsymbol{M}$ is constant in time. Formally we can write

$$\boldsymbol{M}\ddot{\boldsymbol{\xi}} + \boldsymbol{\Omega} \times \boldsymbol{M}\dot{\boldsymbol{\xi}} = \boldsymbol{F}(\boldsymbol{\xi}, \dot{\boldsymbol{\xi}}, \ddot{\boldsymbol{\xi}}, \eta, t) \tag{2}$$

with $\boldsymbol{\xi} \equiv (\xi_1, .., \xi_6)$ the vector of the six rigid body motions, $\boldsymbol{\Omega}$ the angular velocity vector $(\dot{\xi}_4, \dot{\xi}_5, \dot{\xi}_6)$ and the upper dots indicating time (t) derivatives performed along the instantaneous body axes. The cross product is meant to give a six-component vector whose first three components are given by the cross-product of $\boldsymbol{\Omega}$ with the first three components of $\boldsymbol{M}\dot{\boldsymbol{\xi}}$ and the remaining ones by the cross-product of $\boldsymbol{\Omega}$ with the second three components of $\boldsymbol{M}\dot{\boldsymbol{\xi}}$. The generalized forces (forces and moments) $\boldsymbol{F}$ represent the external loads causing the body motions and must be expressed in the (X, Y, Z) reference frame. In equation (2) the loads dependence on the ship motions $\boldsymbol{\xi}$, velocities and accelerations, on the free surface elevation η at the hull, and on the time, is emphasized. Here it is assumed that the buoyancy balances the ship weight in the mean configuration so that they do not appear in $\boldsymbol{F}$ which is given by

$$\begin{aligned} \boldsymbol{F} &= \boldsymbol{F}_{inner} + \boldsymbol{F}_{outer} \\ &= \boldsymbol{F}_{inner} + \boldsymbol{F}_{outer,0} + \boldsymbol{F}_{outer,7} - \boldsymbol{A}_{outer,\infty}\ddot{\boldsymbol{\xi}} - \int_0^t \boldsymbol{h}_{outer}(t-\tau)\dot{\xi}(\tau)d\tau \,. \end{aligned} \tag{3}$$

In the top expression of the right-hand side, the first term represents the nonlinear loads given by the NS solver in a body portion, say S_0, always inside the inner domain. The second term corresponds to the linear loads provided by the linear potential-flow theory in the remaining body portion. It can be decomposed in the sum of the last four terms in the bottom expression of the right-hand side, *i.e.* the excitation (second term), scattering (third term) and radiation loads (fourth and fifth terms). It means that the corresponding pressure terms have been integrated only on the aft portion of the ship. Here $\boldsymbol{A}_{outer,\infty}$ and $\boldsymbol{h}_{outer}$ stand, respectively, for the infinite-frequency added-mass and

Prepared using nmeauth.cls
DOI: 10.1002/nme

impulse-response function matrix associated with the hull portion examined in the outer domain. In the application discussed here only the heave and pitch motions, ξ_3 and ξ_5, are different than zero. As we see, the potential-flow loads solution involves convolution integrals connected with the free-surface memory effects (see [5] and [6]). It means that we have two degrees of coupling: 1) one between the outer and inner domain and 2) the other between loads and motions to be estimated in time domain. It is convenient to choose the inner domain as a cylindrical domain with rectangular cross section and faces parallel to the main axes of the field-solver Cartesian grid, as shown in sketch 5 giving also the main features of the coupling strategy. The hull portion in grey in the sketch

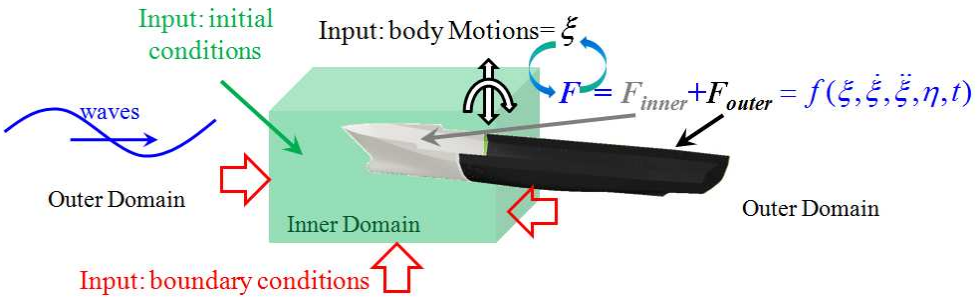

Figure 5. Strong coupling main features: loads partially from the inner and partially from the outer solver. The input information from the outer to the inner solver are also indicated.

represents S_0 where the inner solver estimates the loads, while the rest of the hull in black is where the linear seakeeping solver evaluates the corresponding loads. The motion equations (2) must be solved in time domain and this is done using a second-order Runge-Kutta scheme. Because the loads in the right-hand side depend on the ship acceleration $\ddot{\boldsymbol{\xi}}$ instability problems could arise if this load contribution is relevant compared to the corresponding inertial load. To avoid such problems one should identify an explicit form of the added-mass contribution so that it can be moved on the left-hand side to make better conditioned the system matrix. Therefore as a rough estimate of this load term, $\boldsymbol{A}_\infty\ddot{\boldsymbol{\xi}}$ is summed to the two sides of the equations system (2). Here $\boldsymbol{A}_\infty$ is the infinite-frequency added-mass matrix obtained by the linear potential-flow theory for the whole hull.

Figure 6 shows the flow diagram in the general strong-coupling case. Within the DD the time interval Δt is stated by stability limits and accuracy requirements of the NS solver. In the present

Prepared using nmeauth.cls
DOI: 10.1002/nme

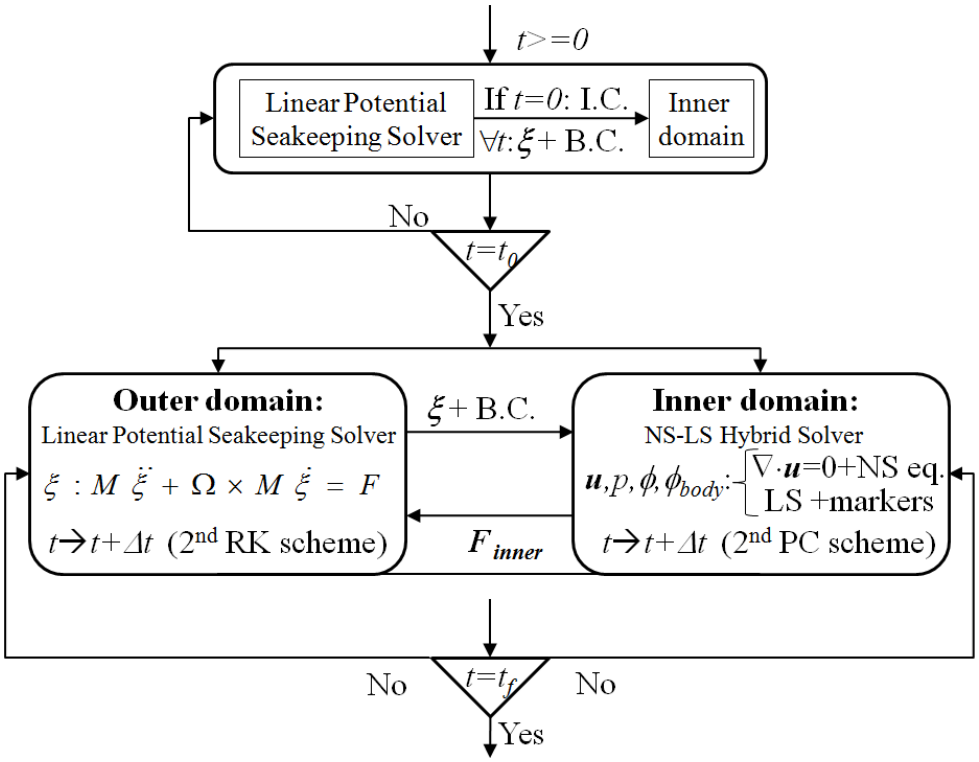

Figure 6. Strong coupling: flow diagram. RK=Runge Kutta. PC=Predictor Corrector. $t = t_0$ is the time of DD starting and $t = t_f$ is the end of the simulation.

implementation the problem starts with the linear potential seakeeping solver up to time $t = t_0$. In this initial interval, a DD strategy with weak-coupling is applied: the inner solver receives the information from the outer solver but it does not provide the loads back. This is useful to correct the initial linear potential-flow solution in time and to achieve a more robust solution in the inner domain when the strong coupling is started. More in detail, the outer domain provides the initial velocity and pressure fields and the initial free surface elevation to the inner domain. Moreover, the boundary conditions are made available along the vertical and bottom boundaries at the time instants required within the Predictor-Corrector integration scheme. It has been found that at $t = t_0 = 10\Delta t$ the strong coupling can switched on without any stability issue. From this time instant on, when integrating from t to $t + \Delta t$, first the outer solver estimates the body motions using a second-order Runge-Kutta scheme. The excitation and scattering loads are estimated at the exact time instant required, while the infinite-frequency added-mass contribution and the convolution integrals are estimated at time t

Prepared using nmeauth.cls
DOI: 10.1002/nme

and kept constant during the motion time-step integration. Finally $\boldsymbol{F}_{inner}$ is estimated at the exact time instant required using a local linear extrapolation based on the two most recent time instants when the NS loads have been calculated. The motions calculated at $t + \Delta t$ are provided to the inner solver as constant to perform the time integration from t to $t + \Delta t$. The boundary conditions in terms of velocity, pressure and free-surface elevation, are provided instead at the time instants used within the Predictor-Corrector scheme. Then at the new time instant the field solver is able to integrate the pressure along the body portion S_0. This provides $\boldsymbol{F}_{inner}(t + \Delta t)$ which will be used to estimate the $\boldsymbol{F}_{inner}$ at the time instants required by the outer solver within the second-order Runge-Kutta scheme for the body-motion equations. This procedure continues until the final time t_f of the simulation. If Δt is very small compared with the time scale of the body motions, say T, to limit the computational time $\boldsymbol{F}_{inner}$ can be estimated every $\gamma\Delta t$ with $\gamma > 1$ and local linear extrapolation is used to guess the inner loads when required by the outer solver. If $T/\gamma\Delta t > 150$, the error committed in doing so is relatively negligible to the numerical error connected with the used solution method. In the present applications, at least $T/\gamma\Delta t = 180$ was used.

The numerical algorithm here explained can be easily extended to more general conditions, as long as we identify adequately the inner and outer domains.

5. INNER-DOMAIN BOUNDARY CONDITIONS: ASSESSMENT

The weak-coupling strategy is used here to assess the proper boundary conditions that must be provided to the NS-LS hybrid solver.

5.1. Vertical inflow boundary portions: overlapping

At the vertical boundary portions, which are upstream relative to the incident-wave propagation, inflow conditions are applied for all variables. More in detail, the potential-flow pressure and free surface elevation are sharply enforced, respectively, for a layer of α_p and α_f cells, to the NS-LS hybrid solver. Differently, the velocity varies linearly from the potential flow to the NS solution within a layer of α_u cells. This means that an overlapping is used for the velocity. The effect of

Prepared using nmeauth.cls
DOI: 10.1002/nme

the overlapping extension is investigated here using the case of a pure wave propagation problem. The (linear) Airy wave solution with propagation direction inclined with respect to the Cartesian grid main axes is enforced at the two upstream sides of the Navier-Stokes domain and the water evolution is studied. A wave propagation not parallel to the grid main axes represents by itself a good test case to check the method capability to preserve the wave properties. The two upstream vertical boundaries, relative to the wave propagation, present a superposition region, where the velocity values are between the linear potential-flow and the NS solution. The boundary portion on the bottom is a simple contact surface, where the linear potential-flow solution is sharply enforced for the velocity (as well as for the pressure). The remaining two vertical boundaries in this example are characterized by outflow boundary conditions, *i.e.* the velocity is obtained by extrapolation from the NS solution (as well as the pressure and the free surface elevation). Figure 7 gives the solution after two periods in terms of the contour levels of the longitudinal velocity and pressure at a plane with constant x and in terms of the free surface configuration. In this case the wave steepness is $kA = 0.12$ and the wave orientation angle relative to the x axis is $\theta = 60^o$. The results show that an overlapping extension of at least six cells is needed to avoid irregular behavior of the velocity which originates at the overlapping and then propagates inside the computational domain. This choice ensures both the bounding of the pressure oscillations that can be induced by the linear-nonlinear inconsistencies and an adequate definition of the interface to calculate the distance function in the narrow band at the interface boundary (see [7]). The inconsistency between the inflow and internal pressure, visible for any value of the overlapping width, does not affect by itself the numerical solution inside the domain, *i.e.* it remains localized near the boundary. Using these results, $\alpha_u = 6$ (cells) is applied in the domain-decomposition strategy for the wave-body interaction problem to interpolate from the potential-flow to the NS solution when inflow condition is enforced for the velocity at the vertical sides of the boundary. Similar studies have shown that $\alpha_f = 6$ and $\alpha_p = 2$ can be used for the free-surface elevation and for the pressure, respectively. The chosen strategy proved to be rather robust also for steeper incident waves reaching freely floating bodies. In particular, the differences due to the inconsistency between linear and nonlinear solution remain localized near

Prepared using nmeauth.cls
DOI: 10.1002/nme

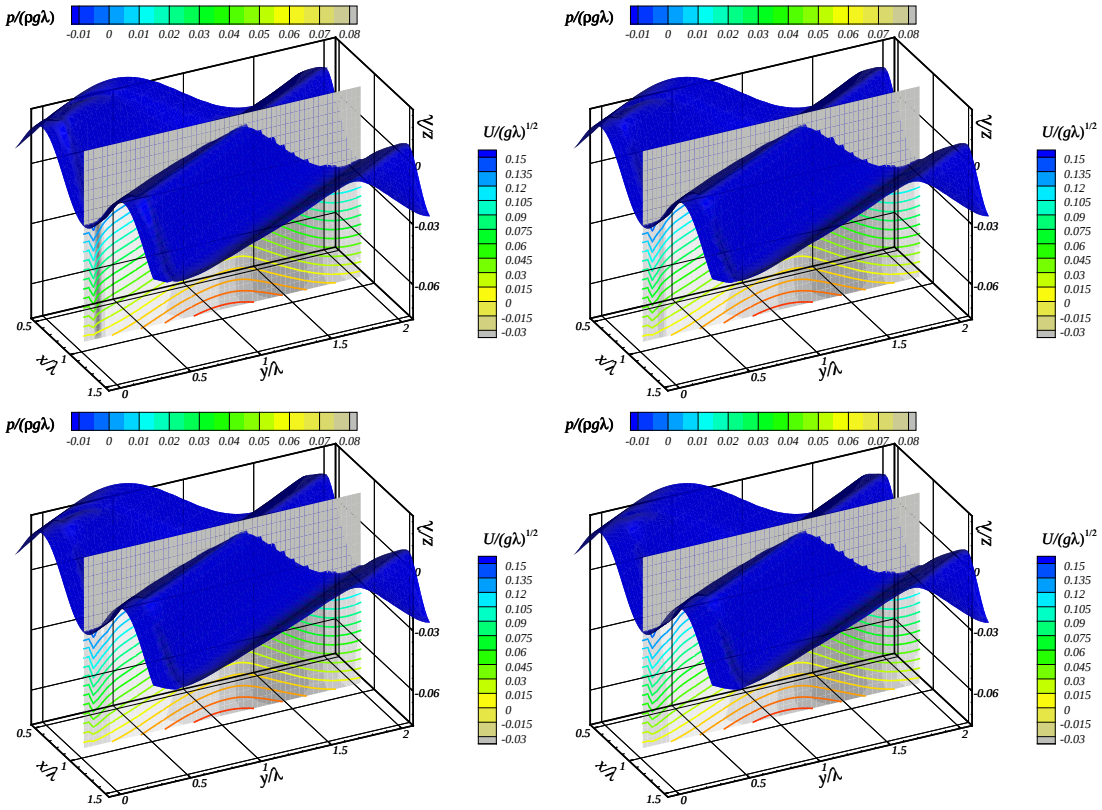

Figure 7. Pure wave propagation problem: effect of overlapping extension $\alpha_u \Delta x$. From left to right and from top to bottom: $\alpha_u = 4$, 5, 6 and 7. Wave steepness $kA = 0.12$ and wave orientation angle relative to the x axis $\theta = 60^o$. Solution after two periods. The small ripples visible on the free-surface are not connected with the numerical solution but due to graphic problems.

the overlapping and do not destroy the flow features inside the Navier-Stokes domain. Naturally such inconsistency becomes less important as the wave steepness reduces. This is shown in figure 8 where an Airy wave with steepness $kA = 0.03$ enters the NS domain with an angle $\theta = 60^o$. In this case, $\alpha_u = 6$ is used for the overlapping extension and the behavior of the solution near this exchange-information region is more regular than for the steeper wave condition and similar to the solution provided by the field solver.

5.2. Downstream boundary portion

At the vertical downstream boundary, inflow conditions are provided for the pressure and the wave elevation, similarly as done at the upstream and side boundaries. For the velocity, three different conditions are checked: outflow, which means that the solution is extrapolated constantly from the

Prepared using nmeauth.cls
DOI: 10.1002/nme

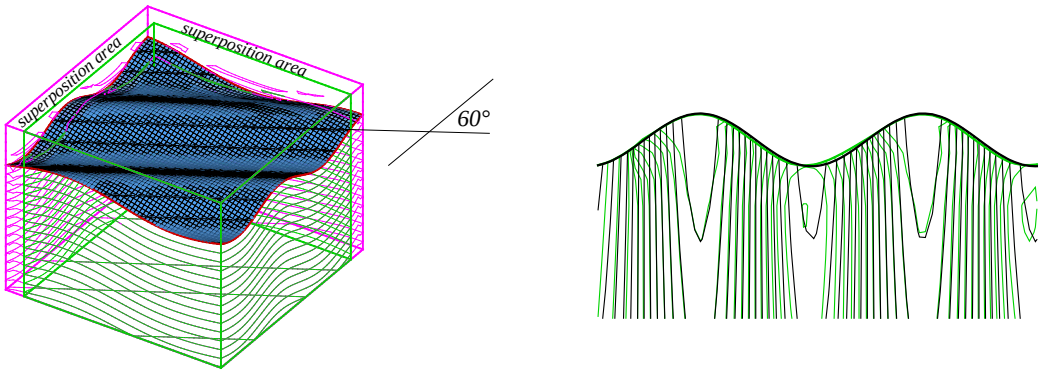

Figure 8. Left: Comparison between theoretical (meshed in black) and numerical free surface (blue shaded) after two wave periods. Pressure contours are plotted on the side of the domain. Right: Comparison between theoretical (black) and numerical (green) contour plots of x-component of the velocity. Wave steepness $kA = 0.03$ and wave orientation angle relative to the x axis $\theta = 60^o$. Solution after two periods. $\alpha_u = 6$.

NS solution; inflow, which means that the solution is enforced to be a linear interpolation between the potential-flow and the NS solution as along the other vertical boundaries; and mixed. The third condition is something between the inflow and outflow conditions (see sketch in figure 9): at the body surface, *i.e.* at the iso-surface $\phi_{body} = 0$, and for a distance less than $3\Delta x$ from it, the outflow condition is applied. For distances greater than three cells the inflow condition is applied. The

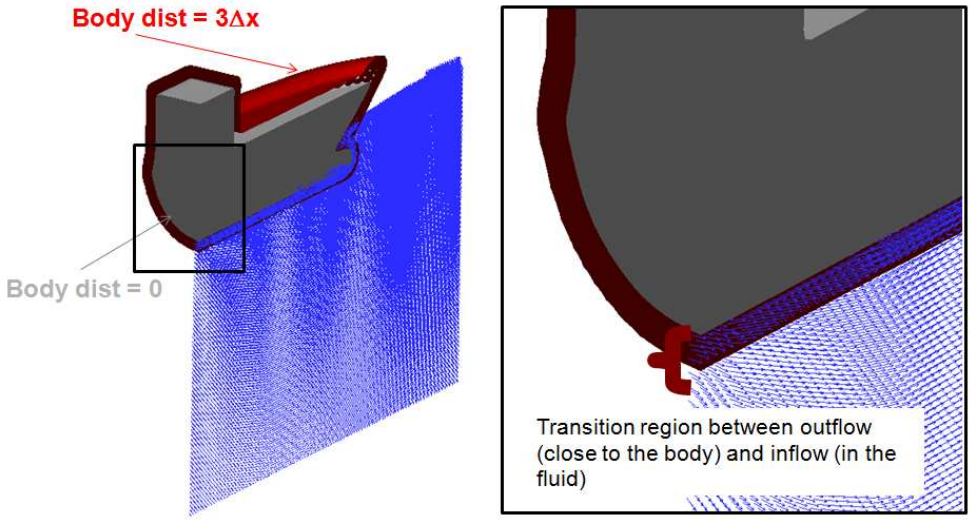

Figure 9. Downstream boundary: mixed condition between inflow and outflow for the velocity.

Prepared using nmeauth.cls
DOI: 10.1002/nme

inflow and mixed conditions are highly more reliable and accurate than the outflow condition. The mixed condition proved to have some advantages with respect to the pure inflow in the case of a body intersecting the inner-domain boundary. The pure potential-flow solution implies a free-slip condition at the body surface while the NS-LS hybrid solver enforces a no-slip condition at the body. A pure inflow condition leads to an inconsistency near the body surface between the inner and outer solutions which could be responsible for fictitious vorticity formation and shedding from the body. The sensitivity of the NS solution to the choice of the downstream boundary condition is investigated next using the problem of an oscillating ambient flow past a circular cylinder.

2D circular cylinder in infinite fluid A simple example to discuss the consequences of the three downstream boundary conditions is sketched in figure 10: a periodic ambient velocity $U\cos(2\pi t/T)$ along x past a 2D fixed rigid circular cylinder. The period of oscillation T and the velocity amplitude are chosen so that the Reynolds and KC numbers are small and correspond to a laminar unseparated flow. In particular $Rn = 2UR/\nu \simeq 10^4$ and $KC = UT/D = 0.8$. The problem is in the (x, y)-plane so that there are no gravity effects. The potential flow solution for the linear problem, *i.e.* with the dynamic pressure $p = -\rho\partial\phi/\partial t$, is

$$\begin{aligned} u &= U\Re[1-(R/z)^2]\,\cos(2\pi t/T) \\ v &= -U\Im[1-(R/z)^2]\,\cos(2\pi t/T) \\ p &= \rho U\Re[z+R^2/z]\,2\pi\sin(2\pi t/T)/T \end{aligned} \tag{4}$$

with $z = x + iy$ the complex coordinate with origin in the cylinder center. This solution is reported in figure 11 in terms of velocity vectors, and contour levels of the pressure and vorticity (ω) fields at the two time instants with zero and maximum ambient velocity, respectively, $t = 19.75T$ and $t = 20T$. Naturally, in this case, ω is null in the fluid. This solution has been provided to the NS solver to study the problem in $x/R \in [-2.5, 2.5]$ and $y/R \in [-3, 0]$. The flow symmetry is enforced at the cylinder center line while at the downstream boundary the inflow is enforced for the velocity. The results are given in the top-left plots of figures 12 and 13, respectively, at $t = 19.75T$ and $t = 20T$. As we see, the no-slip condition causes a flow field with not exactly zero velocity at the

Prepared using nmeauth.cls
DOI: 10.1002/nme

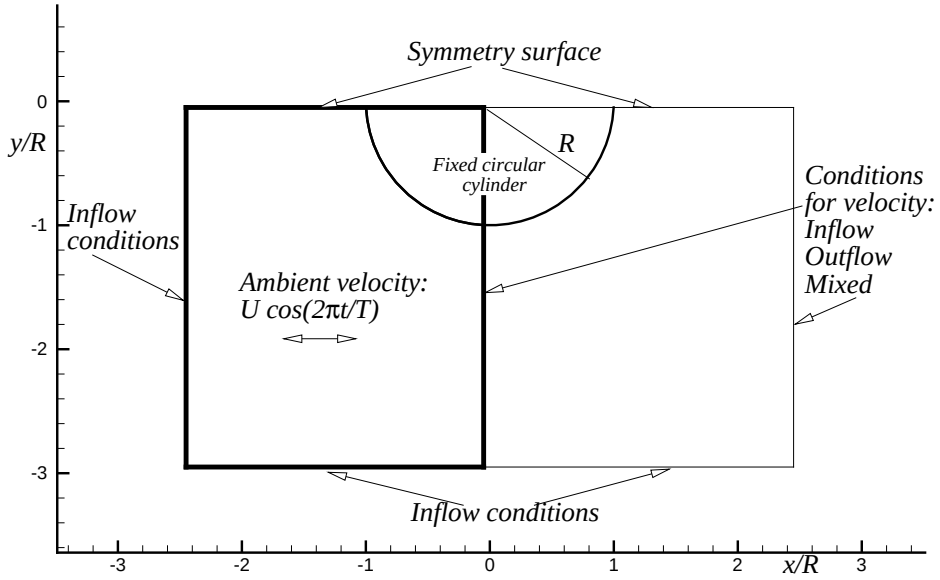

Figure 10. Periodic ambient velocity past a 2D fixed rigid circular cylinder. Sketch of the problem and definition of the NS domains used to solve the problem by enforcing the linear potential-flow solution as input. The thick box represents the short domain, the thin box enclosing it represents the wide domain, for the NS simulations.

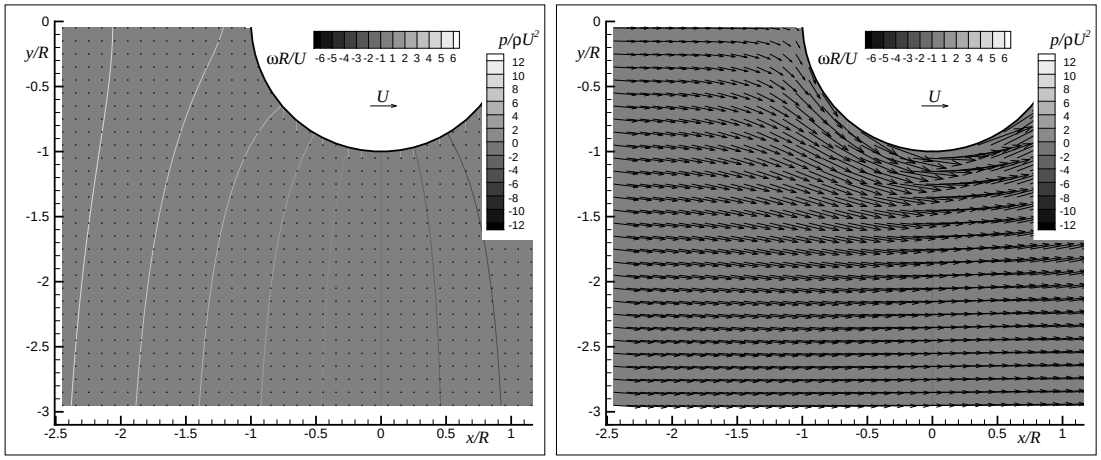

Figure 11. Periodic ambient velocity past a 2D fixed rigid circular cylinder: linear potential-flow solution. Velocity vectors, and contour levels of the pressure and vorticity (ω) fields. From left to right: $t = 19.75T$ and $20T$.

first time instant and not exactly zero pressure at the second time instant. A vorticity is concentrated near the body and will remain there as the flow remains attached in these conditions. The remaining

DOI: 10.1002/nme

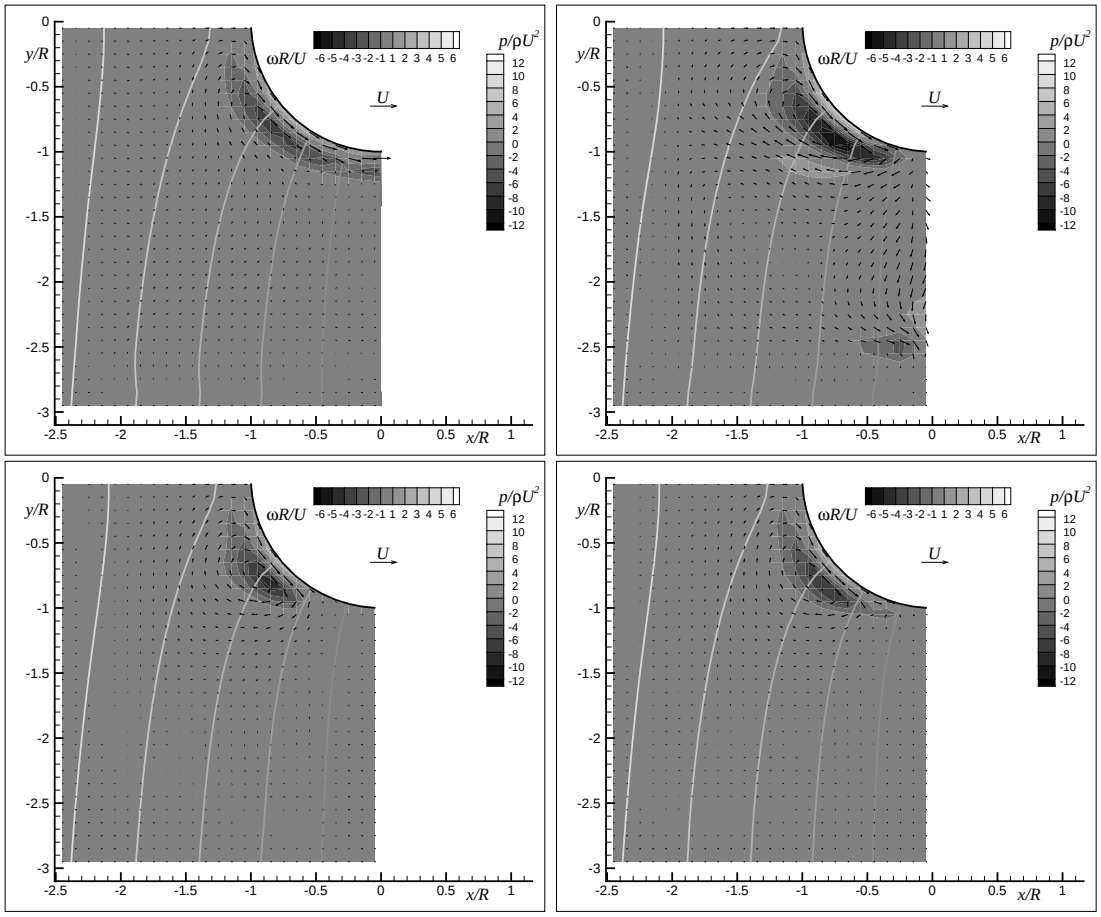

Figure 12. Periodic ambient velocity past a 2D fixed rigid circular cylinder. Downstream boundary: sensitivity to the velocity boundary condition. Top-left: NS solution in $x/R \in [-2.5, 2.5]$ and $y/R \in [-3, 0]$ using inflow condition for the velocity in the downstream boundary. Remaining plots: NS solution in $x/R \in [-2.5, 0]$ and $y/R \in [-3, 0]$ using outflow (top-right), inflow (bottom-left) and mixed (bottom-right) boundary conditions for the velocity in the downstream boundary. Time $t = 19.5T$.

plots of the two figures refer to the outflow, inflow and mixed conditions when the NS solver is applied in a shorter domain with $x/R \in [-2.5, 0]$ and $y/R \in [-3, 0]$ so that the body crosses the downstream boundary. The worst results in terms of velocity and vorticity fields are obtain at the time instant with zero potential-flow velocity, because the flow features are very sensitive to the numerical choices and errors. The worst results are clearly obtained enforcing the outflow condition to the velocity. At this stage, part of the vorticity formed at the body surface entered the fluid and the flow velocity is rather different than the NS solution in the wider domain. The flow features

Prepared using nmeauth.cls
DOI: 10.1002/nme

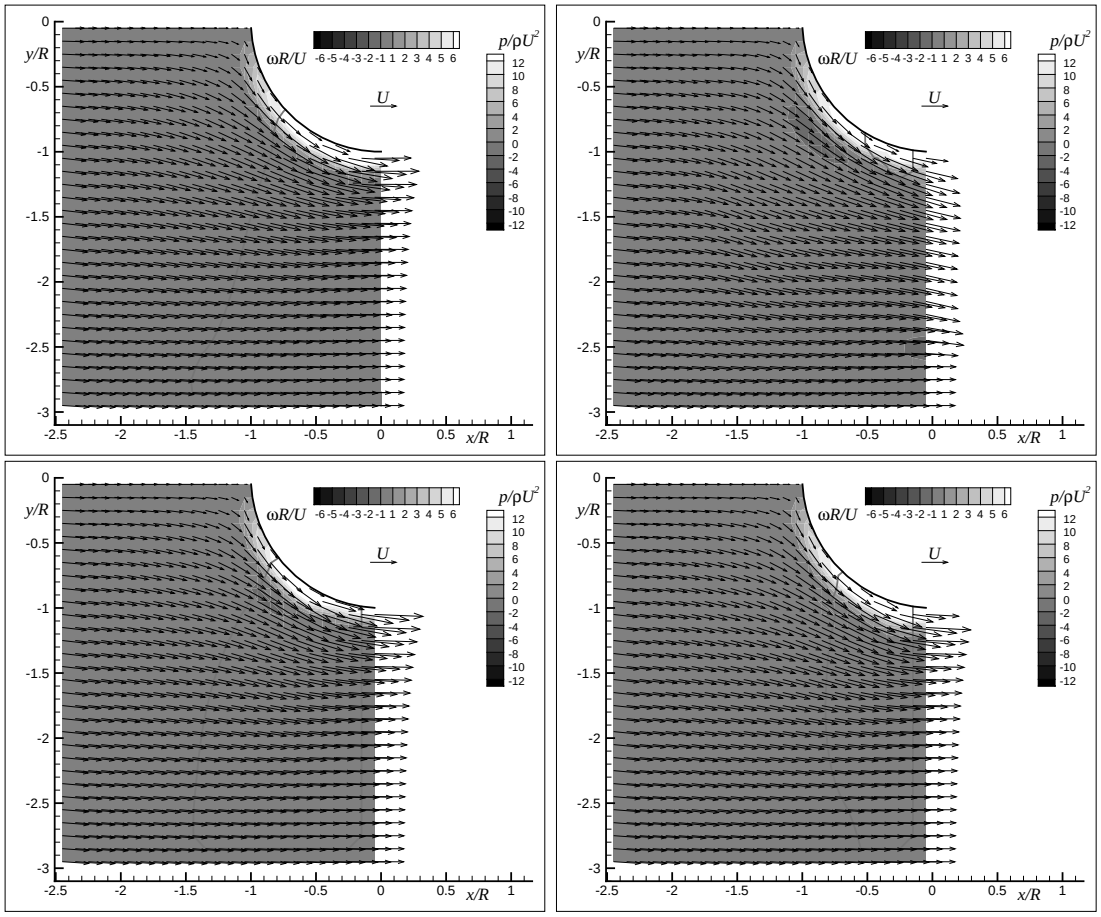

Figure 13. Periodic ambient velocity past a 2D fixed rigid circular cylinder. Downstream boundary: sensitivity to the velocity boundary condition. Top-left: NS solution in $x/R \in [-2.5, 2.5]$ and $y/R \in [-3, 0]$ using inflow condition for the velocity in the downstream boundary. Remaining plots: NS solution in $x/R \in [-2.5, 0]$ and $y/R \in [-3, 0]$ using outflow (top-right), inflow (bottom-left) and mixed (bottom-right) boundary conditions for the velocity in the downstream boundary. Time $t = 20T$.

even far from the body show some unphysical behavior. The inflow and mixed conditions are more physical and similar, but the vorticity level and its detachment from the body surface are slightly more pronounced using the inflow condition. At the second time instant shown, the pressure results are clearly more sensitive to the numerical errors, because the potential-flow solution would predict uniform (and zero) pressure. The results by the inflow and mixed conditions are still competitive but also at this time instant the level of vorticity in the fluid is higher by enforcing the inflow condition.

Prepared using nmeauth.cls
DOI: 10.1002/nme

Moreover near the body surface, towards the downstream boundary, the velocity vectors are more different than enforcing the mixed condition with respect to the NS solution in the wider domain.

The mixed condition, being the most robust among the three examined conditions, has been chosen to investigate more general conditions.

6. APPLICATION TO A PATROL SHIP

Here the DD strategy is applied to the problem of a patrol ship without forward speed and free to oscillate in heave and pitch under the action of incident deep-water regular head-sea waves. The fluid domain is split as shown in the left plot of figure 5, which means that the inner solver is in $x/L \in [0.176, 0.8]$, $y/L \in [-0.252, 0]$ and $z/L \in [-0.317, 0.16]$, with L the ship length. The NS-LS hybrid solver provides the loads on S_0 defined as the ship portion with $x \gtrapprox 0.22$ in the mean configuration because it remains always inside the inner domain in the examined conditions. The weak coupling is used next to assess the validity of the numerical choices made for the inner solver, then the strong coupling is applied.

6.1. Weak coupling

The basic grid discretization used is uniform with $\Delta x = 0.006L$. Left plot of figure 14 shows the effect of using the extrapolation and interpolation techniques for the estimation of the body loads. The discretized body surface obtained using the marching-cube scheme within the interpolation strategy is shown in the right of the same figure. The case refers to a forced-heave problem with period corresponding to a wavelength $\lambda \simeq 1.25L$ and with amplitude $|\xi_3| = 0.1D$, with D the ship draft. It is used to check the reliability of the two load-calculation strategies in case of a moving body. It is evident the more correct behavior of the vertical force acting on S_0 when the interpolation technique is adopted. The extrapolation leads instead to unphysical oscillations even for this simple case with motion parallel to one of the main axes of the computational grid. Such oscillations

Prepared using nmeauth.cls
DOI: 10.1002/nme

represent in general a problem when a strong coupling is considered and the loads from the NS-LS hybrid inner domain are introduced in the motion equations, and even more when dealing with wave-body interactions involving elastic behavior of the structure.

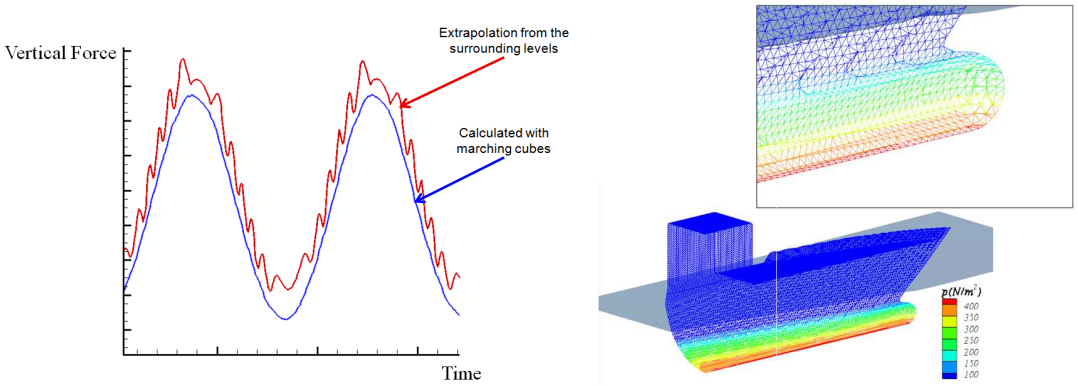

Figure 14. Weak coupling. Left: forced-heave problem. Vertical force on S_0 as estimated by extrapolation and interpolation with marching-cube algorithm. Oscillation period corresponding to a wavelength $\lambda \simeq 1.25L$ and motion amplitude $|\xi_3|/D = 0.1$. $\Delta x/L = 0.006$. Right: triangular discretization of the body surface obtained using the marching-cube scheme.

Figure 15 examines the effect of the downstream boundary condition for the velocity in terms of the vertical force and pitch moment on S_0 in the case of the diffraction problem with incident waves long $\lambda \simeq 1.25L$ and steep $kA = 0.05$. This case has been preferred to a radiation problem because in the latter case the body motions could make more difficult the comparison among the different boundary conditions and because the loads results in the diffraction problem will be more sensitive to numerical inconsistencies connected with the downstream boundary condition. The case is well captured by the linear potential-flow theory due to the small incident wave steepness. Therefore this solution is taken as reference to assess the correctness and accuracy of the numerical solution. From the comparisons, the best results are provided by the mixed condition for the velocity enforced at the downstream boundary. The outflow condition gives the worst solution with large underestimate of the loads amplitude, while the inflow condition introduces a phase error and the related solution appears slightly less smooth than the other results. This is probably due to the formation of fictitious vortical structures at the body surface convected and diffused in time in

Prepared using nmeauth.cls
DOI: 10.1002/nme

the liquid. The mixed condition is therefore applied to investigate also the radiation problems in

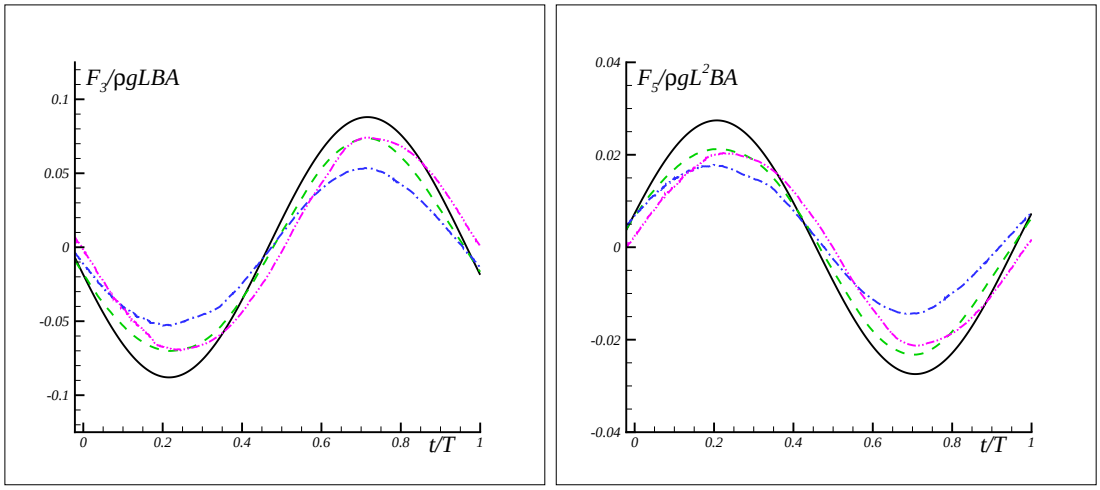

Figure 15. Weak coupling: diffraction problem. Vertical force (left) and pitch moment (right) on S_0. Linear potential solution (solid line) *versus* the numerical solution enforcing the outflow condition (dashed-dotted line), the inflow condition (dashed-dot-dotted line) and the mixed condition (dashed line) for the velocity at the downstream boundary. Incident wavelength $\lambda \simeq 1.25L$ and steepness $kA = 0.05$. T is the incident wave period and L and B are the ship length and beam, respectively, ρ is the water density and g the gravity acceleration. $\Delta x/L = 0.006$.

linear conditions and compared against the linear potential-flow solution. The results for the forced heave and pitch are given in figure 16 and 17, respectively. The forced-heave results show the best agreement, also with respect to the diffraction problem, while the forced-pitch results correspond to the largest discrepancies. This is expected because of the motion not aligned to the main grid axes. Moreover, one must keep in mind that the examined cases are within the linear theory, which means that the motion amplitudes involved are comparable or similar to the grid size, and the loads are estimated only on the portion S_0 of the ship. As a result, the loads are very sensitive to the numerical choices and errors. The forced-pitch motion, representing the most challenging motion for the solver, has been used to assess the method accuracy. The order of accuracy is used as average measure of the numerical error. Let $f(t)$ be a local or global physical quantity that we want to monitor, and let estimate it with the three different discretizations shown in figure 18, *i.e* using $\alpha\Delta x$, with $\alpha = 1, 1/\sqrt{2}$ and 1/2, respectively. For each discretization we can estimate the time

Prepared using nmeauth.cls
DOI: 10.1002/nme

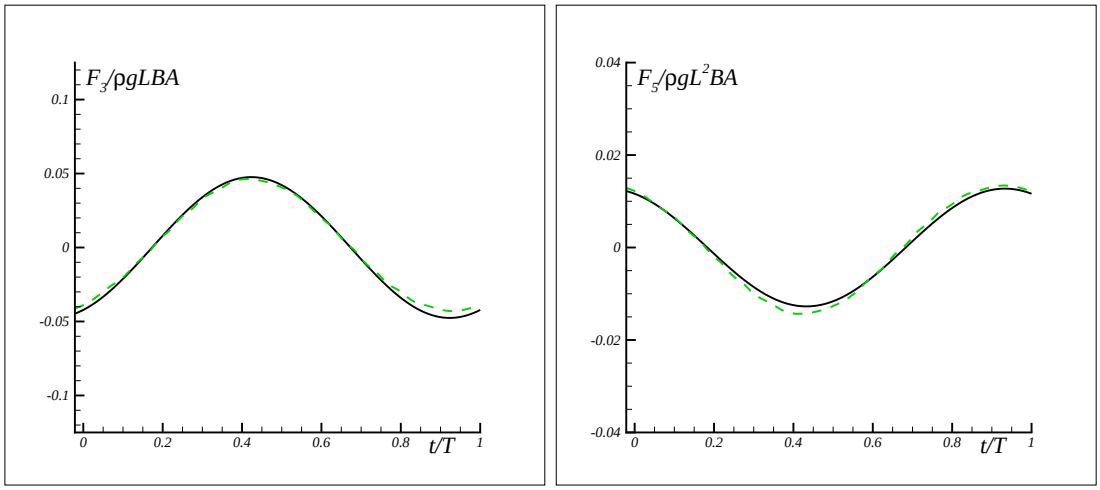

Figure 16. Weak coupling: forced-heave problem. Vertical force (left) and pitch moment (right) on S_0. Linear potential solution (solid line) *versus* the numerical solution enforcing the mixed condition for the velocity at the downstream boundary (dashed line). The oscillation period T corresponds to a wavelength $\lambda \simeq 1.25L$ and the motion amplitude is $|\xi_3|/D = 0.1$. L, D and B are the ship length, draft and beam, respectively, ρ is the water density and g the gravity acceleration. $\Delta x/L = 0.006$.

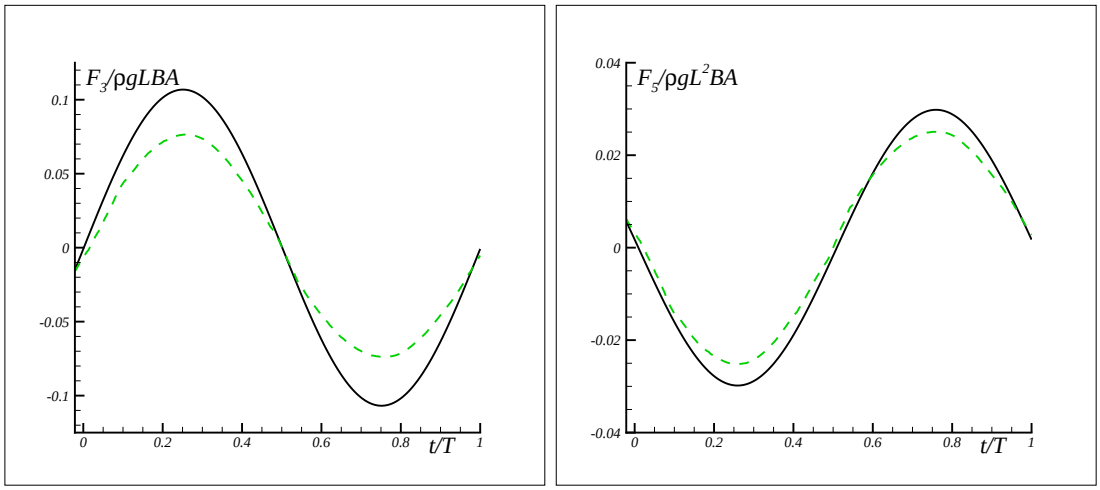

Figure 17. Weak coupling: forced-pitch problem. Vertical force (left) and pitch moment (right) on S_0. Linear potential solution (solid line) *versus* the numerical solution enforcing the mixed condition for the velocity at the downstream boundary (dashed line). The oscillation period T corresponds to a wavelength $\lambda \simeq 1.25L$ and the motion amplitude is $|\xi_5|L/2D = 0.37$. L, D and B are the ship length, draft and beam, respectively, ρ is the water density and g the gravity acceleration. $\Delta x/L = 0.006$.

Prepared using nmeauth.cls
DOI: 10.1002/nme

integral $I_{\alpha\Delta x} = \int_{t_0}^{t_1} f_{\alpha\Delta x}(t)dt$. Then a measure of the numerical accuracy averaged in the time interval $[t_0, t_1]$ can be obtained as

$$OA = \frac{\log[(I_{\Delta x} - I_{\Delta x/2})/(I_{\Delta x/\sqrt{2}} - I_{\Delta x/2})]}{\log(\sqrt{2})}. \tag{5}$$

for the used discretizations. In the specific forced-pitch case, assuming $f(t)$ equal to the vertical force on the ship portion S_0, we get $OA = 2.45$ and taking it as the pitch moment on the same surface, we have $OA = 2.52$. These values are consistent with the second-order accuracy of the present scheme and indicate a convergence rate slightly faster than two.

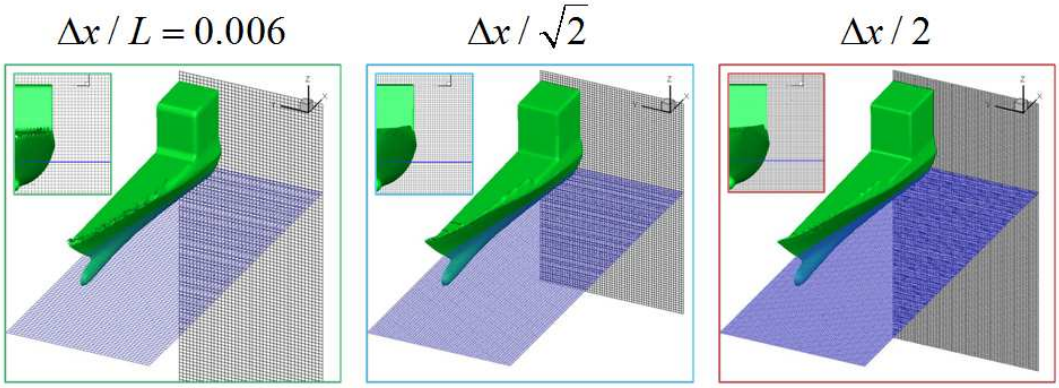

Figure 18. Weak coupling. Convergence study for the forced pitch problem. Three discretizations with uniform mesh size. The oscillation period T corresponds to a wavelength $\lambda \simeq 1.25L$ and the motion amplitude is $|\xi_5|L/2D = 0.37$. L and D are the ship length and draft, respectively.

6.2. Strong coupling

The radiation and diffraction problems investigated in the weak-coupling case correspond to the seakeeping solution provided by linear potential-flow theory in the case of incident waves long $\lambda \simeq 1.25L$ and with small steepness $kA = 0.05$. Figure 19 shows the comparison between the heave and pitch motions given by this reference solution and the DD strategy using the strong coupling approach. The heave is positive upwards and the pitch is positive with bow downwards. The DD algorithm provides stable results which are in good agreement with the linear solution. This confirms the correctness of the numerical choices of building up the compound solver. Next

Prepared using nmeauth.cls
DOI: 10.1002/nme

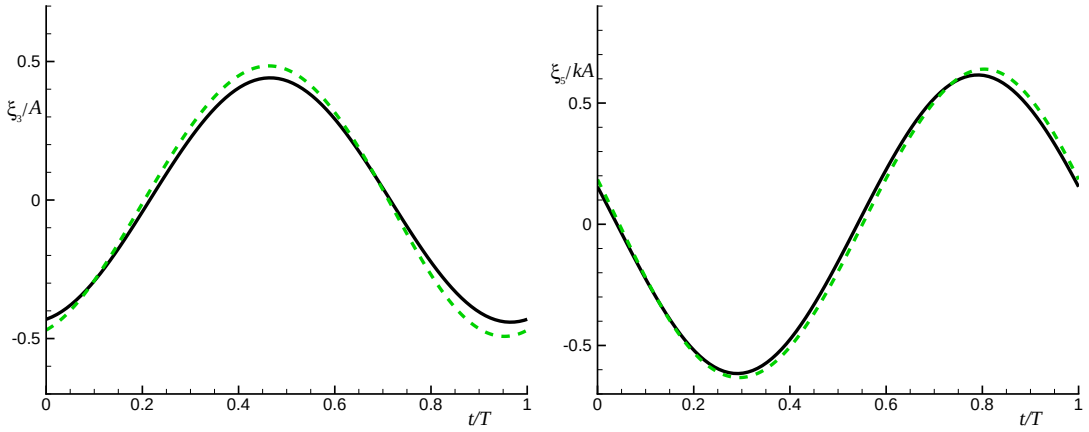

Figure 19. Seakeeping problem: comparison between the linear potential-flow solution (solid line) and the DD strong-coupling results (dashed line) in terms of heave and pitch motions. Incident wavelength $\lambda \simeq 1.25L$ and steepness $kA = 0.05$. $\Delta x/L = 0.006$ with L the ship length. T is the incident-wave period.

figures examine the case of incident waves with the same wavelength and $kA \simeq 0.22$. The examined λ is in the vertical-motion resonance region and the wave-body interaction causes in the physical case small impact events at the bow bottom and sides, and water shipping, as documented by the experimental observations in [11]. These model tests are used here for validating the numerical solver globally and locally. The basic grid discretization with $\Delta x/L = 0.006$ is used to perform the simulations. The examined patrol ship has a very thin bulwark protecting partially the deck and a vertical superstructure at a short distance from the end of the bulwark (see figure 20). Using this discretization does not allow to reproduce the deck protection as a continuous wall because it is thinner than the grid size, therefore the bulwark was made as thick as Δx. This represents an error source in terms of amount of shipped water, as discussed later.

Global analysis: flow evolution The ship motion and water evolution from the model tests and as predicted by the DD are given in figure 21. Qualitatively the results agree globally well at the different stages of the wave-body interaction. Also the water-on-deck occurrence is captured, but the used discretization does not allow to estimate correctly the amount of shipped water. The numerical results underestimate clearly this quantity.

Prepared using nmeauth.cls
DOI: 10.1002/nme

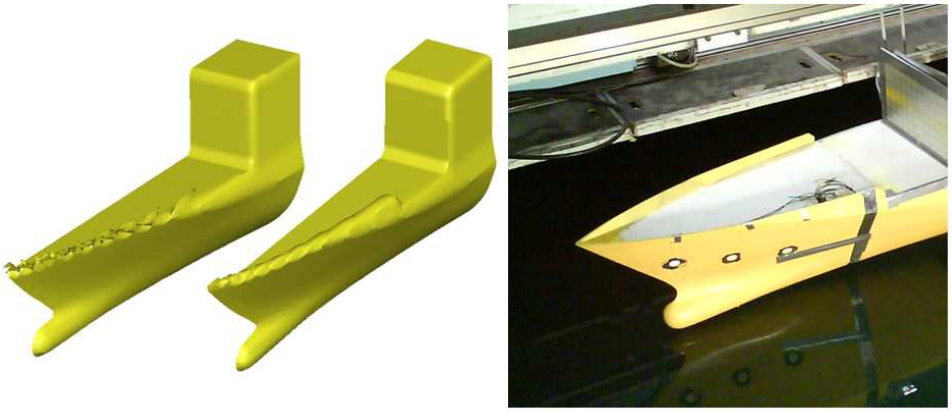

Figure 20. Discretization of the ship portion inside the inner domain using a grid size $\Delta x/L = 0.006$ without (left) and with thickening the bulwark (center). The physical ship model is given in the right.

Global analysis: ship motions The comparison in terms of the heave and pitch motion is provided in figure 22. For the experiments two curves are given, they refer to the same test run with one curve at a temporal distance of about 15 incident-wave periods from the other. The differences between the two experimental curves give a rough measure of the involved experimental error and are connected with seiching occurrence in the towing tank. This refers to the development of a shallow-water standing wave leading to an envelope of the propagating waves. As expected such phenomenon affects mostly the heave motion which is directly connected with the incident-wave amplitude. The error in the pitch motion is instead limited because ξ_5 is affected by the incident-wave steepness, *i.e.* by the wave slope which is less sensitive to the seiching occurrence. The comparison between the measurements performed with an optical system (Krypton) and the numerical results for the heave shows differences within the experimental error while the disagreement with the pitch appears quite relevant near the motion peak. Positive pitch means bow downwards which corresponds to the phase of water-on-deck occurrence for this case. A possible explanation of the discrepancies could be given by the fact that the solver underestimates the amount of shipped water and therefore underpredicts the pitch-motion increase under the weight of the liquid onto the deck. Another possible cause of the differences could be connected with nonlinear wave-body interaction effects in the ship loads. The fully nonlinear inner solver estimates $\boldsymbol{F}_{inner}$ only in a ship portion with $x \gtrapprox 0.22$

Prepared using nmeauth.cls
DOI: 10.1002/nme

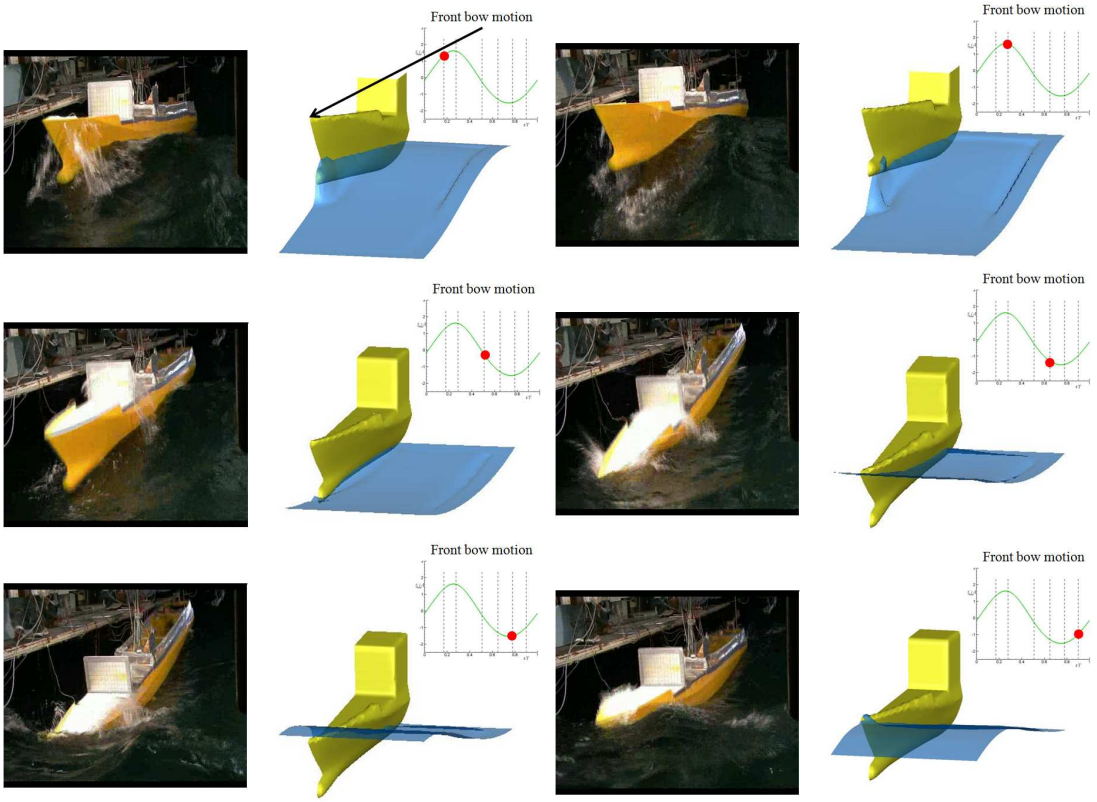

Figure 21. Seakeeping problem: experimental (left in each plot) and DD results (right in each plot) in terms of ship motion and water evolution. Time increases from left to right and from top to bottom and the graph in the right of each plot gives the numerical position of the forward bow at each plotted time instant. Incident wavelength $\lambda \simeq 1.25L$ and steepness $kA \simeq 0.22$. $\Delta x/L = 0.006$ with L the ship length. T is the incident-wave period.

but nonlinear effects could be relevant in a larger portion of the vessel. To check these aspects, the simplified 3D DD by Greco and Lugni [12] is used. This couples a weakly-nonlinear seakeeping solver with a shallow-water method for the evolution of the shipped water. The results provided by this solver appear closer to the experiments in terms of pitch peak. When applying this simplified DD strategy setting to zero the loads induced by the shipped water, the pitch peak is not much affected. So, this suggests that nonlinear effects along the hull can be the major reason for the discrepancies. The present DD has then been applied including the second-order effects in the incident waves and in the Froude-Kriloff and hydrostatic loads contributions provided by the outer solver in the aft portion of the vessel. One must note that this is inconsistent because we have only accounted for

Prepared using nmeauth.cls
DOI: 10.1002/nme

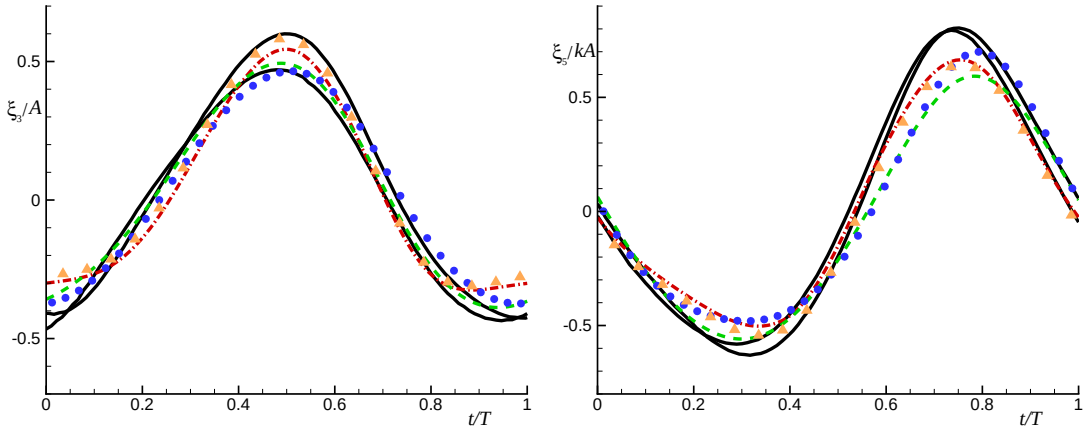

Figure 22. Seakeeping problem: heave and pitch motions as measured (two solid curves in each plot) and predicted by the present DD (dashed line), by the simplified DD with shallow-water solver on the deck (dashed-dotted line), by the simplified DD without water-on-deck loads (triangles), and by the present DD with second-order effects associated with the incident waves, and with the Froude-Kriloff and hydrostatic loads on the outer ship portion (circles). Incident wavelength $\lambda \simeq 1.25L$ and steepness $kA \simeq 0.22$. $\Delta x/L = 0.006$ with L the ship length. T is the incident-wave period.

some second-order effects. For instance we did not consider the contributions from the radiation and scattering phenomena. This approximated version of the 3D weakly-nonlinear seakeeping solver coupled with the NS-LS hybrid method is just used to understand what is physically missing. In terms of pitch peak the results are closer to the experiments than as provided by the original DD; while the trough prediction is slightly worsened. This highlights a sensitivity to the nonlinear effects in the hull loads and suggests that they could be an important reason for the discrepancies. For this incident wavelength, the model tests show that nonlinear effects are important also for smaller steepnesses (see [12]). The results for the smallest value of kA studied experimentally are reported in figure 23 in terms of heave and pitch motions and show limited seiching effects. In this case there is no water on deck and the heave motion is dominated by linear potential-flow phenomena, except for near the peak. Present DD is closer to the model tests in this case and coincides with the solution obtained including second-order effects connected with the incident waves, and with the Froude-Kriloff and hydrostatic loads. The approximated DD by Greco and Lugni [12] looses a bit near the heave through. For the pitch, the numerical curves are consistent and underestimate slightly

Prepared using nmeauth.cls
DOI: 10.1002/nme

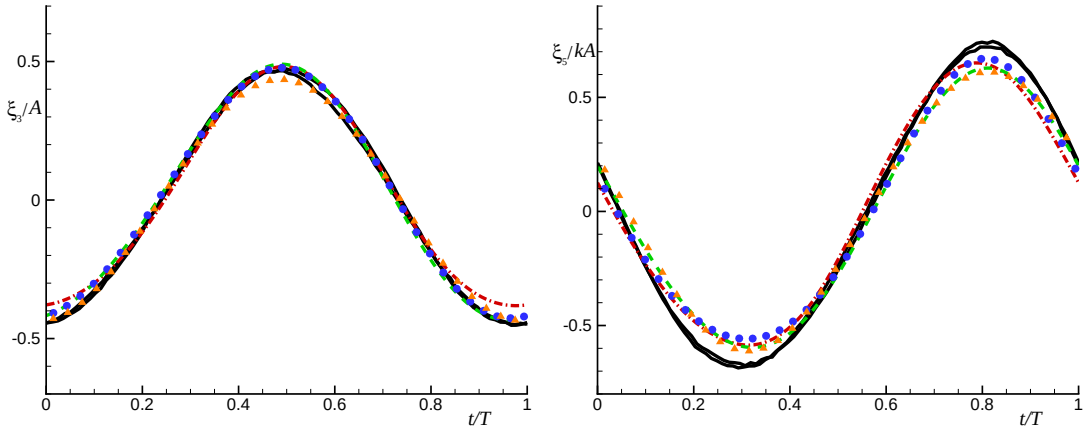

Figure 23. Seakeeping problem: heave and pitch motions as measured (two solid curves in each plot) and predicted by the present DD (dashed line), by the simplified DD with shallow-water solver on the deck (dashed-dotted line), by the present DD with second-order effects associated with the incident waves, and with the Froude-Kriloff and hydrostatic loads on the outer ship portion (circles) and by the linear potential-flow theory (triangles). Incident wavelength $\lambda \simeq 1.25L$ and steepness $kA \simeq 0.091$. $\Delta x/L = 0.006$ with L the ship length. T is the incident-wave period.

the measurements. We can not rule out the possibility that some physical effects are missing in the used flow models, but the discrepancies could also be due to an effect of the adopted experimental set up. This explanation would be consistent with the fact that also at the largest kA examined in figure 22 the model tests showed larger pitch motion amplitudes than all numerical results.

Local analysis: pressure on the hull Since the numerical solution with $\Delta x/L = 0.006$ does not predict the correct amount of shipped water, the evolution of the flow onto the deck and the induced pressure on the vessel are not analyzed here and left for a future work once the inner solver has been made more efficient and then using a sufficiently fine discretization. In the following the pressures measured in the bow region, on the bottom and at the side of the ship, are examined.

Despite the relatively course grid used for the simulation, the present DD (coupling the linear potential-flow solver with the nonlinear NS-LS method) is able to capture the main features of the pressure time evolutions at the two locations examined in figure 24. One must note however some oscillatory behavior of the numerical pressure suggesting the need for a more detailed description

Prepared using nmeauth.cls
DOI: 10.1002/nme

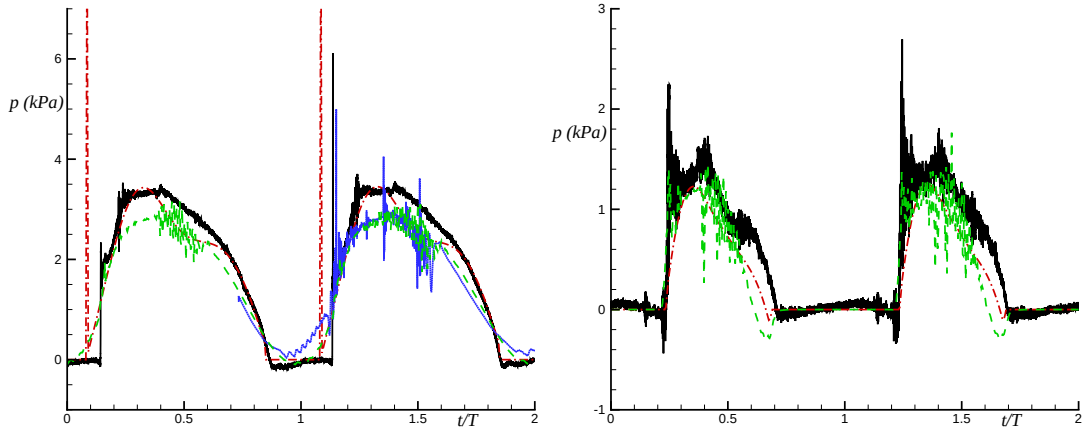

Figure 24. Seakeeping problem: pressure at the bottom (station 18) and at the side (station 19) of the hull. The measurements (solid line) are compared with the present DD (dashed line, $\Delta t/T \simeq 0.0005$) and with the simplified DD with shallow-water solver on the deck (dash-dotted line). The dotted line for the bottom pressure represents the present DD with Δt five times smaller (i.e. $\Delta t/T \simeq 0.0001$) obtained restarting the numerical simulation from the solution with $\Delta t/T \simeq 0.0005$. Incident wavelength $\lambda \simeq 1.25L$ and steepness $kA \simeq 0.22$. $\Delta x/L = 0.006$ with L the ship length. T is the incident-wave period.

of the local flow. The impact occurring at the ship bottom is not handled by the simulation with $\Delta t/T \simeq 0.0005$ due to the short duration of the phenomenon which shows also a stochastic behavior from the measurements (see [11]). A decrease of a factor five of the time step is suitable to model the impact and provides a pressure peak comparable with the second experimental peak shown in the figure. The simplified DD (coupling a shallow-water approximation on the deck with a weakly-nonlinear potential flow seakeeping solver) includes a local Wagner-type solution and is able to detect the impact occurrence but overpredicts the pressure peak for the shown events. Present pressure on the side of the hull is more consistent with the measurements than the results from the simplified DD. In particular it shows a fast pressure rise, right after the pressure sensor becomes wet, due to the water-hull impact. This impact phenomenon is affected by the flare in this portion of the vessel and is completely disregarded by the simplified DD showing mainly a hydrostatic increase of the pressure. The examined results are promising however, for a comprehensive assessment of the method, numerical convergence should be examined also for this ship seakeeping problem. Due

Prepared using nmeauth.cls
DOI: 10.1002/nme

to the high computational cost required, this is left to future work after a proper improvement of the solver efficiency.

7. CONCLUSIONS AND FUTURE WORK

A 3D Domain-Decomposition (DD) strategy has been developed. This couples a linear potential seakeeping solver, in an outer domain, with a nonlinear Navier-Stokes solver based on a Projection method that combines a Finite-Difference scheme with a Level-Set technique for the free-surface evolution and with a hybrid method made of the Eulerian Level-Set approach and Lagrangian markers for the body motion, in an inner domain. The main features of the coupled solvers have been outlined, special development of the inner solver connected with the DD strategy was described. Weak and strong coupling approaches have been examined and the numerical choices in terms of inner domain boundary conditions were addressed. Verification studies of the different solver features have been presented. The application to a patrol ship was used for further verification of the numerical choices by examining radiation and diffraction problems and applying the weak-coupling approach. Then the strong coupling was applied to investigate the seakeeping problem of the vessel interacting with regular head-sea waves. The solver was successfully verified by comparison against the fully linear potential-flow solution in the case of incident waves with small steepness and validated against model tests in the case of steeper waves. The next steps concern the improvement of the code efficiency. Figure 25 gives the time profiling of the solver when using the marching-cube scheme for the loads time integration. As we can see the major cost is connected with the solution of the fluid-momentum equations, then we have the marching-cube algorithm cost that can be reduced using the approach by Colicchio in [8], For example in the case of mesh with $\Delta x/L = 0.006$, the CPU time required for the loads calculation can be reduced of a factor about 1000. Finally the costs of the body motion and the free-surface evolution which are comparable. A substantial improvement of the numerical efficiency, can be obtained moving from an incompressible to a pseudo-compressible solver. In this way the solution of the Poisson equation is avoided and the solver can easily be parallelized. This approach is preferred to the use

Prepared using nmeauth.cls
DOI: 10.1002/nme

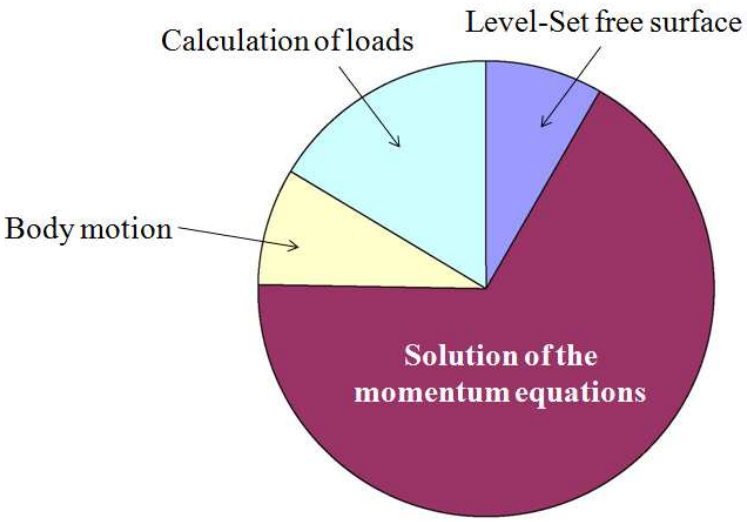

Figure 25. Time profiling: relative cost of the main parts of the solver.

of a multigrid approach to solve the Poisson equation, because the latter is more closely related to the specific geometry of the problem and so less elastic. At present the pseudo-compressible solver is under development with promising results in terms of accuracy and efficiency for internal-flow problems.

ACKNOWLEDGEMENTS

This research activity is supported by the Centre for Ships and Ocean Structures (CeSOS), NTNU, Trondheim, within the ”Violent Water-Vessel Interactions and Related Structural Loads” project.

REFERENCES

1. Colicchio G., Greco M. and Faltinsen O.M. A BEM-Level Set Domain Decomposition Strategy for Nonlinear and Fragmented Interfacial Flows. *J. for Numerical Methods in Engineering*. 2006; **67** (10):1385-1419.
2. Colicchio G., Greco M. and Faltinsen O.M. Domain-Decomposition Strategy for Marine Applications with Cavities Entrapments. *J. of Fluids and Structures.* 2011; **27** (4).
3. Bulgarelli U., Carcaterra A., Landrini M. and Lugni L. Mooring System Optimization for Vessel in Waves. *OMAE 97*, Yokohama, Giappone. 1997.
4. Newman J.N. *Marine hydrodynamics.* MIT Press, Cambridge, Massachusett. 1977.

Prepared using nmeauth.cls
DOI: 10.1002/nme

5. Cummins W.E. The impulse response function and ship motions. *Schiffstechnik.* 1962; **9** (47): 101–109.
6. Ogilvie T.F. Recent progress toward the understanding and prediction of ship motions. 5^{th} *Symposium on Naval Hydrodynamics.* Office of Naval Research-Department of the Navy, Washington D.C. 1964; 3-128.
7. Colicchio G. Violent disturbance and fragmentation of free surfaces. *Ph.D. thesis*. University of Southampton,Southampton, UK. 2004.
8. Colicchio G. A hybrid Eulerian-Lagrangian technique to model arbitrary body motions. *Technical Report CNR-INSEAN*. 2011.
9. Colicchio G., Landrini M. and Chaplin J. R. Level-Set Computations of Free Surface Rotational Flows. *Journal of Fluids Engineering*. 2005; **127** (6):1111-1121.
10. Enright D., Fedkiw R., Ferziger J. and Mitchell I. A hybrid particle level-set method for improved interface capturing. *J. of Computational Physics.* 2002; **325**: 377-397.
11. Greco M., Bouscasse B. and Lugni C. 3D seakeeping analysis with water-on-deck and bottom-slamming occurrence: experiments and physical investigation. *submitted to J. of Fluids and Structures.* 2011.
12. Greco M. and Lugni C. 3D seakeeping analysis with water-on-deck and bottom-slamming occurrence: numerical solver. *submitted to J. of Fluids and Structures.* 2011.

Prepared using nmeauth.cls
DOI: 10.1002/nme